S1 Complete description of Eq. (7)

We consider the model depicted in Fig. 1 (panel a). Linear transport in and out of each grid cell is defined by a rate constant $k = U/L = 1/\tau'$ (Jacob, 1999). We assume that the system is in steady state and write a mass balance for the mass of the trace gas in the jth grid cell (m_j):

$$\frac{dm_j}{dt} = 0 = Ax_j + km_{j-1} - km_j \tag{S1}$$

$$m_j = \frac{A}{k}x_j + m_{j-1} \tag{S2}$$

$$m_j = A\tau' x_j + m_{j-1} \tag{S3}$$

The area A converts the flux from units of mass per area per time to mass per time. Equation (S3) is recursive with $m_0 = m_c$ corresponding to the mass of the trace gas at the BC. We then write the non-recursive expression:

$$m_j = A\tau'\left(x_1 + x_2 + \cdots + x_j\right) + m_c. \tag{S4}$$

We convert from mass m_j to concentration y_j using

$$m_j = \frac{M_{\mathrm{X}}}{M_{\mathrm{air}}}\frac{PA}{g}y_j \tag{S5}$$

where M_{X} and M_{air} are the molar masses of the trace gas and air, respectively; P is the atmospheric pressure, assumed constant; A is the grid cell area; and g is gravitational acceleration. We rewrite Eq. (S4) in concentration units as

$$y_j = \alpha\tau'\left(x_1 + x_2 + \cdots + x_j\right) + c \tag{S6}$$

where c is the concentration of the trace gas at the BC and

$$\alpha = \frac{M_{\mathrm{air}}}{M_{\mathrm{X}}}\frac{g}{P}. \tag{S7}$$

We then differentiate y_j with respect to x_i to obtain the jth row and ith column of the Jacobian matrix $\mathbf{K}_{ji}$:

$$\mathbf{K}_{ji} = \frac{dy_j}{dx_i} = \begin{cases} \alpha\tau', & i \le j \\ 0, & i > j \end{cases}. \tag{S8}$$

This is a lower diagonal matrix with constant values given $\tau = \alpha\tau'$ as described by Eq. (7):

$$\mathbf{K} = \alpha\tau' \begin{bmatrix} 1 & & & \\ 1 & 1 & & \\ \vdots & \vdots & \ddots & \\ 1 & 1 & \dots & 1 \end{bmatrix} \tag{S9}$$

If grid cells are combined, the corresponding elements of the Jacobian matrix are added together.

S2 Complete definition and derivation of Eq. (9)

We will show that Eq. (10) is equal to $\Delta\hat{\boldsymbol{x}} = -\mathbf{G}\boldsymbol{\varepsilon}_{\mathrm{C}}$ in the extremes of $R \ll 1$ and $R \gg 1$. We define the Jacobian matrix $\mathbf{K}$ to be lower diagonal with constant values given by τ so that $\mathbf{K} = \tau\mathbf{L}$ where $\mathbf{L} \in \mathbb{R}^{n\times n}$ is the lower diagonal matrix of ones (Supplement S1). The prior and observing system covariance matrices $\mathbf{S}_{\mathrm{A}}$ and $\mathbf{S}_{\mathrm{O}}$ are assumed to be diagonal matrices with constant values of σ_{A}^2 and $\sigma_{\mathrm{O}}^2/m_g$, respectively. We define $\boldsymbol{\varepsilon}_{\mathrm{C}} = \varepsilon_{\mathrm{C}}\mathbf{1}$ where $\mathbf{1}$ is the vector of ones. We then write the background-induced posterior error vector as

$$\Delta\hat{\boldsymbol{x}} = -\mathbf{G}\boldsymbol{\varepsilon}_{\mathrm{C}} = -(\mathbf{S}_{\mathrm{A}}^{-1} + \mathbf{K}^{\mathrm{T}}\mathbf{S}_{\mathrm{O}}^{-1}\mathbf{K})^{-1}\mathbf{K}^{\mathrm{T}}\mathbf{S}_{\mathrm{O}}^{-1}\boldsymbol{\varepsilon}_{\mathrm{C}} \tag{S10}$$

$$= -\frac{\tau\varepsilon_{\mathrm{C}}}{\sigma_{\mathrm{O}}^2}\left(\frac{1}{\sigma_{\mathrm{A}}^2}\mathbf{I}_n + \frac{\tau^2}{\sigma_{\mathrm{O}}^2}\mathbf{L}^{\mathrm{T}}\mathbf{L}\right)^{-1}\mathbf{L}^{\mathrm{T}}\mathbf{1} \tag{S11}$$

$$= -(\tau^{-1}\varepsilon_{\mathrm{C}})R(\mathbf{I}_n + R\mathbf{L}^{\mathrm{T}}\mathbf{L})^{-1}\mathbf{L}^{\mathrm{T}}\mathbf{1} \tag{S12}$$

where R is the error ratio defined by Eq. (6). Rearranging yields

$$(\mathbf{L}^{\mathrm{T}})^{-1}\Delta\hat{\boldsymbol{x}} + R\mathbf{L}\Delta\hat{\boldsymbol{x}} = -(\tau^{-1}\varepsilon_{\mathrm{C}})R\mathbf{1}. \tag{S13}$$

The inverse of the $\mathbf{L}^{\mathrm{T}}$ is known to be a bi-diagonal matrix with diagonal entries equal to 1 and super-diagonal entries equal to -1. We write out the rows of this equation:

$$\Delta\hat{x}_1 - \Delta\hat{x}_2 + R\Delta\hat{x}_1 = -(\tau^{-1}\varepsilon_{\mathrm{C}})R \tag{S14}$$

$$\Delta\hat{x}_2 - \Delta\hat{x}_3 + R\Delta\hat{x}_1 + R\Delta\hat{x}_2 = -(\tau^{-1}\varepsilon_{\mathrm{C}})R \tag{S15}$$

$$\Delta\hat{x}_3 - \Delta\hat{x}_4 + R\Delta\hat{x}_1 + R\Delta\hat{x}_2 + R\Delta\hat{x}_2 = -(\tau^{-1}\varepsilon_{\mathrm{C}})R \tag{S16}$$

$$\vdots \quad = \quad \vdots$$

$$\Delta\hat{x}_{n-1} - \Delta\hat{x}_n + R\Delta\hat{x}_1 + R\Delta\hat{x}_2 + \cdots + R\Delta\hat{x}_{n-1} = -(\tau^{-1}\varepsilon_{\mathrm{C}})R \tag{S17}$$

$$\Delta\hat{x}_n + R\Delta\hat{x}_1 + R\Delta\hat{x}_2 + \cdots + R\Delta\hat{x}_{n-1} + R\Delta\hat{x}_n = -(\tau^{-1}\varepsilon_{\mathrm{C}})R \tag{S18}$$

We form an equivalent set of linear equations by taking pairwise differences of Eqs. (S14 – S18) and appending Eq. (S14). This is equivalent to multiplying Eq. (S13) by $\mathbf{L}^{-1}$, which is a bi-diagonal matrix with diagonal entries equal to 1 and sub-diagonal entries equal to -1. This allows us to rewrite Eqs. (S14 – S18) as:

$$(R+1)\Delta\hat{x}_1 - \Delta\hat{x}_2 = -(\tau^{-1}\varepsilon_{\mathrm{C}})R \tag{S19}$$

$$-\Delta\hat{x}_{i-2} + (R+2)\Delta\hat{x}_{i-1} - \Delta\hat{x}_i = 0, \qquad i = 3, \ldots, n \tag{S20}$$

$$-\Delta\hat{x}_{n-1} + (R+2)\Delta\hat{x}_n = 0. \tag{S21}$$

We recognize Eq. (S20) as a discrete second-order recurrence relation with characteristic equation

$$z^2 - (R+2)z + 1 = 0 \tag{S22}$$

which has roots

$$\rho_1 = \frac{(R+2) + \sqrt{(R+2)^2 - 4}}{2}, \qquad \rho_2 = \frac{(R+2) - \sqrt{(R+2)^2 - 4}}{2}. \tag{S23}$$

These roots are distinct provided that $R \neq 0$. Therefore, for $j = 1, \ldots, n$, the elements $\Delta\hat{x}_j$ will take the form

$$\Delta\hat{x}_j = b_1\rho_1^{j-1} + b_2\rho_2^{j-1}, \tag{S24}$$

where the coefficients b_1 and b_2 will be determined by Eqs. (S19) and (S21). These equations now respectively become

$$(R+1)(b_1+b_2) - (b_1\rho_1 + b_2\rho_2) = -(\tau^{-1}\varepsilon_C)R \tag{S25}$$

$$-[b_1\rho_1^{n-2} + b_2\rho_2^{n-2}] + (R+2)[b_1\rho_1^{n-1} + b_2\rho_2^{n-1}] = 0. \tag{S26}$$

We will re-write this in matrix form

$$\begin{bmatrix} R+1-\rho_1 & R+1-\rho_2 \\ (R+2)\rho_1^{n-1} - \rho_1^{n-2} & (R+2)\rho_2^{n-1} - \rho_2^{n-2} \end{bmatrix} \begin{bmatrix} b_1 \\ b_2 \end{bmatrix} = \begin{bmatrix} -(\tau^{-1}\varepsilon_C)R \\ 0 \end{bmatrix}, \tag{S27}$$

which we can invert to obtain

$$\begin{bmatrix} b_1 \\ b_2 \end{bmatrix} = \begin{bmatrix} R+1-\rho_1 & R+1-\rho_2 \\ (R+2)\rho_1^{n-1} - \rho_1^{n-2} & (R+2)\rho_2^{n-1} - \rho_2^{n-2} \end{bmatrix}^{-1} \begin{bmatrix} -(\tau^{-1}\varepsilon_C)R \\ 0 \end{bmatrix} \tag{S28}$$

$$= \frac{1}{\boldsymbol{\Delta}} \begin{bmatrix} (R+2)\rho_2^{n-1} - \rho_2^{n-2} & -[R+1-\rho_2] \\ -[(R+2)\rho_1^{n-1} - \rho_1^{n-2}] & R+1-\rho_1 \end{bmatrix} \begin{bmatrix} -(\tau^{-1}\varepsilon_C)R \\ 0 \end{bmatrix} \tag{S29}$$

$$= -\frac{(\tau^{-1}\varepsilon_C)R}{\boldsymbol{\Delta}} \begin{bmatrix} (R+2)\rho_2^{n-1} - \rho_2^{n-2} \\ -[(R+2)\rho_1^{n-1} - \rho_1^{n-2}] \end{bmatrix}, \tag{S30}$$

where $\boldsymbol{\Delta}$ is the discriminant

$$\boldsymbol{\Delta} \coloneqq [R+1-\rho_1][(R+2)\rho_2^{n-1} - \rho_2^{n-2}] - [R+1-\rho_2][(R+2)\rho_1^{n-1} - \rho_1^{n-2}]. \tag{S31}$$

We now have the full expression for the values $\Delta\hat{x}_j$ in terms of R:

$$\Delta\hat{x}_j = [b_1 \quad b_2] \begin{bmatrix} \rho_1^{j-1} \\ \rho_2^{j-1} \end{bmatrix} \tag{S32}$$

$$= -\frac{(\tau^{-1}\varepsilon_C)R}{\boldsymbol{\Delta}} \left([(R+2)\rho_2^{n-1} - \rho_2^{n-2}]\rho_1^{j-1} - [(R+2)\rho_1^{n-1} - \rho_1^{n-2}]\rho_2^{j-1} \right). \tag{S33}$$

We now consider the asymptotics for large and small R.

S2.1 Asymptotics: Large R

Upon inspection, for large values of R, we note that ρ_1 is asymptotically equal to $R+2$. We can approximate ρ_2 to the first order. If we consider the function $f(z) = \sqrt{z}$, then

$$f(z+dz) \approx f(z) + f'(z)dz = \sqrt{z} + \frac{1}{2}z^{-1/2}dz. \tag{S34}$$

Thus, for large values of R, we have

$$\sqrt{(\mathrm{R}+2)^2-4} \approx \sqrt{(R+2)^2} + \frac{1}{2}[(R+2)^2]^{-1/2}(-4) \tag{S35}$$

$$= (R+2) - 2(R+2)^{-1}. \tag{S36}$$

Substituting this into our expression for ρ_2 shows that it is asymptotically equal to $(R+2)^{-1}$ for large R. Correspondingly, $\boldsymbol{\Delta}$ asymptotically becomes

$$\boldsymbol{\Delta} \approx [R+1-(R+2)]\left[(R+2)(R+2)^{-(n-1)} - (R+2)^{-(n-2)}\right]$$
$$-[R+1-(R+2)^{-1}][(R+2)(R+2)^{n-1} - (R+2)^{n-2}] \tag{S37}$$

$$= -[(R+2)^{-n+2} - (R+2)^{-n} + 2] - [R+1-(R+2)^{-1}][(R+2)^n - (R+2)^{n-2}] \tag{S38}$$

$$\approx -(R+1)[(R+2)^n - (R+2)^{n-2}] \tag{S39}$$

and

$$-\frac{(\tau^{-1}\Delta c)R}{\boldsymbol{\Delta}} \approx \frac{-(\tau^{-1}\varepsilon_{\mathrm{C}})R}{-(R+1)[(R+2)^n - (R+2)^{n-2}]} \tag{S40}$$

$$\approx (\tau^{-1}\varepsilon_{\mathrm{C}})(R+2)^{-n}. \tag{S41}$$

Therefore, when R is large, $\Delta\hat{x}_j$ is approximately

$$\Delta\hat{x}_j \approx (\tau^{-1}\varepsilon_{\mathrm{C}})(R+2)^{-n}\Big(\left[(R+2)(R+2)^{-(n-1)} - (R+2)^{-(n-2)}\right](R+2)^{j-1}$$
$$-[(R+2)(R+2)^{n-1} - (R+2)^{n-2}](R+2)^{-(j-1)}\Big) \tag{S42}$$

$$\approx (\tau^{-1}\varepsilon_{\mathrm{C}})(R+2)^{-n}\left(-[(R+2)^n - (R+2)^{n-2}](R+2)^{-(m-1)}\right) \tag{S43}$$

$$\approx -(\tau^{-1}\varepsilon_{\mathrm{C}})(R+2)^{-j+1} \tag{S44}$$

$$\approx -(\tau^{-1}\varepsilon_{\mathrm{C}})R^{-j+1} \tag{S45}$$

which matches Eq. (9).

S2.1 Asymptotics: Small R

For $R \to 0$, we now have the approximation

$$\sqrt{(\mathrm{R}+2)^2-4} = \sqrt{4R+R^2} \tag{S46}$$

$$\approx \sqrt{4R} \tag{S47}$$

$$= 2\sqrt{R}. \tag{S48}$$

This allows us to approximate ρ_1 and ρ_2 (Eq. (S23)) as

$$\rho_1 \approx \frac{(\mathrm{R}+2)+2\sqrt{\mathrm{R}}}{2} \approx \frac{2+2\sqrt{R}}{2} = 1+\sqrt{R} \tag{S49}$$

$$\rho_2 \approx \frac{(\mathrm{R}+2)-2\sqrt{\mathrm{R}}}{2} \approx \frac{2-2\sqrt{R}}{2} = 1-\sqrt{R}. \tag{S50}$$

We can furthermore employ the linear approximations for powers of ρ_1 and ρ_2:

$$\rho_1^{\mathrm{N}} \approx 1+\mathrm{N}\sqrt{R} \tag{S51}$$

$$\rho_2^{\mathrm{N}} \approx 1-\mathrm{N}\sqrt{R}. \tag{S52}$$

Now, examining the terms in our expression for the determinant $\boldsymbol{\Delta}$ (Eq. (S31)), we have

$$\mathrm{R}+1-\rho_1 \approx -\sqrt{R} \tag{S53}$$

$$\mathrm{R}+1-\rho_2 \approx \sqrt{R} \tag{S54}$$

$$(R+2)\rho_2^{n-1}-\rho_2^{n-2} \approx (R+2)\big(1-(n-1)\sqrt{R}\big)-\big(1-(n-2)\sqrt{R}\big) \tag{S55}$$

$$\approx 2\big(1-(n-1)\sqrt{R}\big)-\big(1-(n-2)\sqrt{R}\big) \tag{S56}$$

$$= 1-n\sqrt{R} \tag{S57}$$

$$(R+2)\rho_1^{n-1}-\rho_1^{n-2} \approx (R+2)\big(1+(n-1)\sqrt{R}\big)-\big(1+(n-2)\sqrt{R}\big) \tag{S58}$$

$$\approx 2\big(1+(n-1)\sqrt{R}\big)-\big(1+(n-2)\sqrt{R}\big) \tag{S59}$$

$$= 1+n\sqrt{R}. \tag{S60}$$

This allows us to approximate $\boldsymbol{\Delta}$ as

$$\boldsymbol{\Delta} \approx -\sqrt{R}\big[1-n\sqrt{R}\big]-\sqrt{R}\big[1+n\sqrt{R}\big] \tag{S61}$$

$$= -2\sqrt{R}, \tag{S62}$$

and consequently,

$$-\frac{(\tau^{-1}\varepsilon_{\mathrm{C}})R}{\boldsymbol{\Delta}} \approx \frac{1}{2}(\tau^{-1}\varepsilon_{\mathrm{C}})\sqrt{R}. \tag{S63}$$

Therefore, for small R, our expression for $\Delta\hat{x}_j$ now becomes approximately

$$\Delta\hat{x}_j \approx \frac{1}{2}(\tau^{-1}\varepsilon_{\mathrm{C}})\sqrt{R}\big(\big[1-n\sqrt{R}\big]\rho_1^{j-1}-\big[1+n\sqrt{R}\big]\rho_2^{j-1}\big) \tag{S64}$$

$$\approx \frac{1}{2}(\tau^{-1}\varepsilon_{\mathrm{C}})\sqrt{R}\big(\big[1-n\sqrt{R}\big]\big[1+(j-1)\sqrt{R}\big]-\big[1+n\sqrt{R}\big]\big[1-(j-1)\sqrt{R}\big]\big) \tag{S65}$$

$$= \frac{1}{2}(\tau^{-1}\varepsilon_{\mathrm{C}})\sqrt{R}\big(-2n\sqrt{R}+2(j-1)\sqrt{R}\big) \tag{S66}$$

$$= -(\tau^{-1}\varepsilon_{\mathrm{C}})(n-j+1)R \tag{S67}$$

which matches Eq. (9).

S3 Definition of periodic boundary conditions

We define a BC perturbation f as a function of time t

$$f(t) = b + A\sin\left(\frac{2\pi\omega t}{t_{max}}\right) \tag{S68}$$

where b is the y-intercept, A is the amplitude, ω is the number of periods over the simulation duration (including the spin-up and inversion), and t_{max} the last simulated time step in the inversion. We define base values of $b = 1900$ ppb, $A = 10$ ppb, and $\omega = 2$. We then separately vary the y-intercept from 1900 ppb to 1920 ppb, the amplitude from 5 ppb to 15 ppb, and the period number from 1 to 5. All inversions use varying wind speeds.

Table S1: Model configuration for simulation experiments

Model parameter	One-dimensional model	Two-dimensional model
Transport model	One-dimensional model[a] with constant[b] and varying[c] wind speeds	GEOS-Chem[g]
Model domain	20 grid cells	Permian basin, Texas (28.75°N to 34.75°N, 99°W to 106.6875°W)
Model resolution	25 km	$0.25° \times 0.3125°$
True emissions	30 ppb d^{-1} [d]	EDF inventory and Express Extension of the Gridded EPA inventory[h]
True boundary condition	1900 ppb	TROPOMI-based boundary conditions[i]
Spin-up[e]	150 hours	April 2020
Simulation duration	150 hours	May 2020
Number of pseudo-observations	1000	Domain: 4431 Buffer zone: 6391[j]
Pseudo-observation distribution	Uniform in time and space[f]	Averaged TROPOMI methane observations for May 2020[k]
Pseudo-observation error statistics	Mean: 0 ppb Standard deviation: 8 ppb	Mean: 0 ppb Standard deviation: 10.5 ppb[l]

[a] Advection is solved using the Lax-Wendroff scheme in the first $n-1$ grid cells and an upstream scheme for the last grid cell (Brasseur and Jacob, 2017). The model time step is defined so that the maximum Courant number equals 1. The model is initialized at steady state.
[b] The constant wind speed is $U = 5$ m s^{-1}.
[c] The varying wind see-saws between 3 and 7 m s^{-1} at 1 m s^{-1} increments for each time step over 20 hours.
[d] True emissions are constant in time and space.
[e] As is standard in regional inversions, we use a model spin-up to ensure that the background is unbiased with respect to the true BC.
[f] Pseudo-observations are generated by sampling each grid cell's atmosphere at 50 regular intervals over the simulation period.
[g] GEOS-Chem is driven by the GEOS-FP meteorological data from the NASA's Global Modeling and Assimilation Office (GMAO).
[h] True oil and gas emissions are defined by the Environmental Defense Fund (EDF) high-resolution Permian basin inventory for 2019 (Zhang et al., 2020) while all emissions from all other sectors are given by the Express Extension of the Gridded EPA inventory for 2020 (Maasakkers et al., 2023)
[i] We use TROPOMI-based smoothed BCs from the Integrated Methane Inversion (IMI) to generate the true BC concentrations. We calculate the BC concentrations $\boldsymbol{c}$ following the definition of the linearized forward model $F(\boldsymbol{x}) = \mathbf{K}\boldsymbol{x} + \boldsymbol{c}$ (Section 2.1) where F is the GEOS-Chem forward model driven by the true BCs, $\boldsymbol{x}$ is a vector of the IMI default emissions, and $\mathbf{K}$ is the Jacobian matrix generated from the IMI.
[j] Following the IMI, we average the observations over hourly GEOS-Chem grid cells. These counts represent the number of averaged observations over the inversion domain of interest and buffer zone (used only for the buffer method).
[k] The TROPOMI observations are averaged on the $0.25° \times 0.3125°$ model grid for each hour of the inversion.
[l] We generate random, uncorrelated errors with the error statistics shown here for each individual observation. The error statistics correspond to the non-transport observing system error assumed by the IMI (Estrada et al., 2024; Chen et al., 2023). To account for the decrease in error associated with averaging the observations, we reduce the mean error for each hourly grid cell by the square root of the observation count.

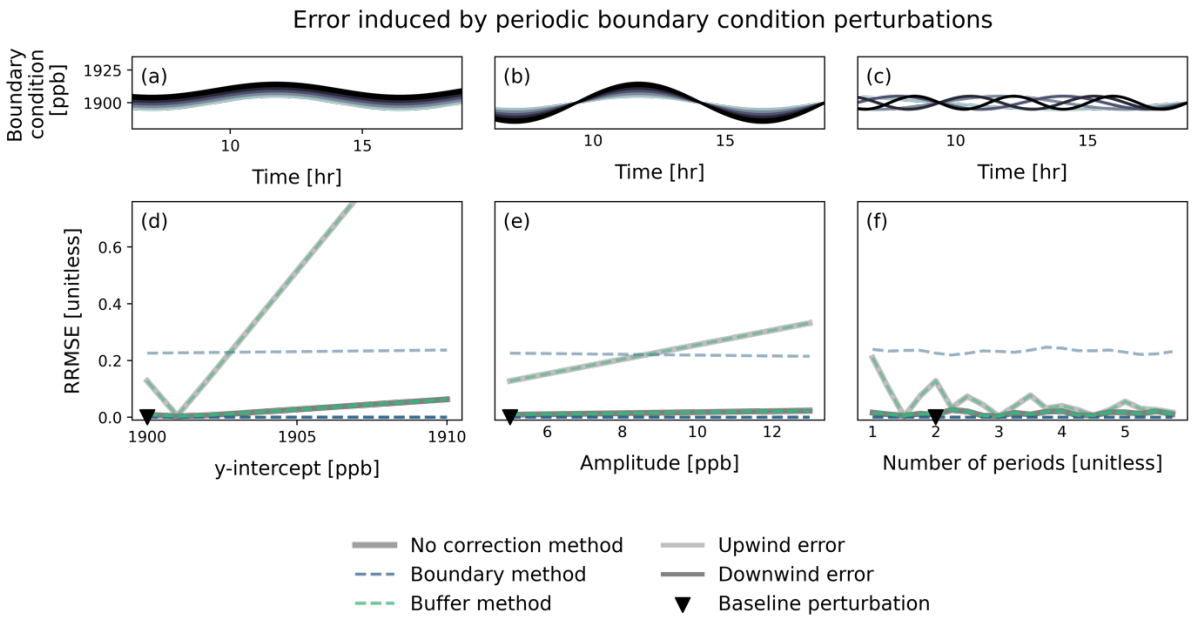

Figure S1: Sensitivity of posterior flux estimates from a one-dimensional inverse model to periodic BC biases using different BC correction methods. Different periodic BC biases are applied to the one-dimensional inverse model by varying the y-intercept (a), amplitude (b), and number of periods over the simulation duration (including the spin-up and inversion; c) of a periodic function. The influence of these BC biases on the posterior fluxes is shown as a function of these parameters (d, e, and f, respectively) as quantified by the relative root mean square error (RRMSE) of the difference between inversions solved with the true and biased BCs. The RRMSE is normalized by the mean prior fluxes and is calculated separately for the upwind and downwind grid cells, defined as the first seven and last thirteen grid cells, respectively, of the 20 grid cells in the one-dimensional domain. The effect of no BC correction mechanism (true error), the boundary method, and the buffer method is also shown.